INTERACTIONS OF THE INTRAGROUP MEDIUM IN TRANSFORMING GALAXY MORPHOLOGIES

An Undergraduate Research Scholars Thesis

by

JONATHAN MONROE

Submitted to Honors and Undergraduate Research
Texas A&M University
in partial fulfillment of the requirements for the designation as

UNDERGRADUATE RESEARCH SCHOLAR

Approved by
Research Advisor: Dr. Kim-Vy Tran

May 2015

Major: Physics
Mathematics

TABLE OF CONTENTS

ABSTRACT

Interactions of the Intragroup Medium in Transforming Galaxy Morphologies. (May 2015)

Jonathan Monroe
Department of Physics and Astronomy
Department of Mathematics
Texas A&M University

Research Advisor: Dr. Kim-Vy Tran
Department of Physics and Astronomy

We utilize high resolution data from Hubble Space Telescope (HST) to study the role of the group environment in galaxy evolution. The majority of galaxies in the universe fall into this regime, and thus are of paramount importance in our understanding of the general evolutionary structure of galaxies. Much work has gone into observing and classifying the effect of the cluster environment on a galaxy's characteristics, but the question remains what role progenitors to this environment (namely groups) play in this change. We conclude that the particular subject of our study has well replicated the effects of the cluster environment. It has uniform characteristics which, while not as dramatic with the cluster regime, are nonetheless consistent with the expected observations of clusters.

ACKNOWLEDGMENTS

I would like to acknowledge Tammis Sherman and Dr. Duncan MacKenzie for their support of standardizing the Undergraduate Research Scholars thesis through the use of LaTeX.

I would also like to acknowledge Mark Senn and Purdue University for allowing me to base this UGR thesis off of the PUThesis template. The ability to use a familiar interface was greatly appreciated, and I was able to accomplish much more than starting from scratch.

Finally, I would like to acknowledge my advisor, Dr. Kim-Vy Tran, for her invaluable input, instruction and support throughout this study. This study would have never left the ground if not for her hard work and expertise.

NOMENCLATURE

HST	Hubble Space Telescope
ICM	Intracluster Medium
ISM	Interstellar Medium
RPS	Ram Pressure Stripping
SG	Supergroup
UV	Ultraviolet
ACS	Advanced Camera for Surveys
WFC3	Wide Field Camera 3

CHAPTER I
INTRODUCTION

A great deal of work has gone into understanding the characteristics of galaxy clusters, but there has been relatively little insight into what role groups play in these characteristics. Several dynamical processes have been observed in and simulated for cluster environments, but such analysis has not yet been applied to the group regime. As the progenitors of cluster environments, these objects provide insight into the uniqueness of the cluster regime's ability to produce the kind of effects hitherto observed. Do group proto-clusters have the ability to reproduce these effects, or are they specifically limited to cluster-scale interactions? I.e. what is the lower bound for these dynamics?

I.1 Physical Processes

In order to understand what role the group environment plays in a galaxy's evolution we must first understand what the uninfluenced, natural evolution of (field) galaxies. As a galaxy evolves, it coalesces cold gas into stars. This process requires cold gas because the kinetic energy of molecules at higher temperatures tends to prohibit particles from binding together into the proper conditions to form stars. This gas comes from reservoirs in the ISM and from the external medium in the form of cold flows accreting onto the galaxy. As this process transpires a variety of sources begin to dilute the cold gas regions with influxes of hot gas. Older and more massive stellar populations begin ejecting media through stellar pulsation and sometimes catastrophically as supernovae. AGN activity also substantially heats gas (preferentially in the galactic core) within the galaxy. These processes are integral to galactic quenching while the influx of cold gas flowing back into galaxy drives additional star formation. Thus the environmental gas-richness directly influences a galaxies evolution.

The morphology of a field galaxy, then, depends to some extent on how gas-rich its surroundings are and how efficiently the galaxy transforms this gas into stars. Spiral galaxies tend towards higher percentage gas content than ellipticals, and though this distinction doesn't drive morphological transformation it does present a relationship between environmental characteristics and observed morphology. Spirals are preferentially found in the field as opposed to in group (or cluster) environments [1]. Thus morphology does not give us an explicit characteristic of groups/clusters, but it can give us some insight into the role of the group regime, especially with particularly disturbed morphologies.

The ram pressure stripping (RPS) model asserts that as a galaxy in-falls to the cluster center the dense intracluster medium (ICM) acts as a drag force which strips low density regions in the galactic disk, leaving higher densities in both the core and disk intact yet compressed(Gunn & Gott 1972)[2]. This process influences star formation and morphology by stripping out existing gas (strangulation) and preventing the inflow of additional gas (starvation). This loss of gas tends to quench star formation in the long term and alters morphology by displacing stars as the shock front moves through the galaxy.

(Owers et al. 2012)[3] identified several examples of this kind of stripping within Abell 2744, a major merging cluster at $z \sim 0.31$. These galaxies have an asymmetric structure with clear streams of stars outflowing away from the group center. These kinds of galaxies, shown in Figure I.1, are clear examples of this kind of stripping taking place. Under more extreme circumstances (Kenney et al. 2012) [4] found the galaxy in Figure I.1 in the Virgo Cluster- a particularly RPS-inducing environment. Its rapid infall velocity and the high ICM density shredded large portions of the galaxy and coalesced them into smaller collections of star-forming gas. These new clouds of gas were still influenced by the ICM interaction and formed back-flow streams, resembling fireballs popping out of the galaxy. Such observations have been confirmed by n-body hydrodynamical simulations[5].

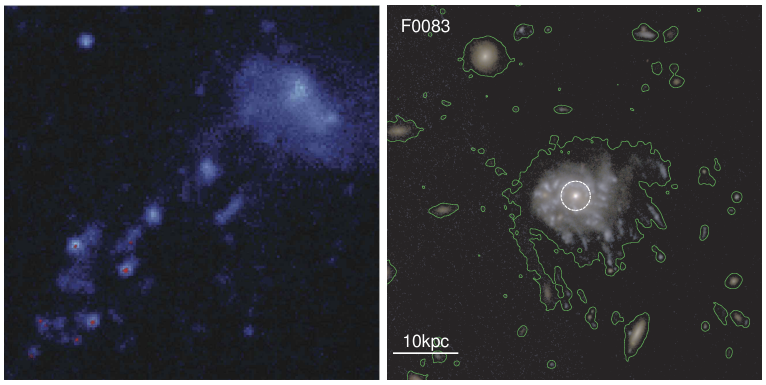

Fig. I.1. Examples of “jellyfish” and “fireball” galaxy morphologies as observed in Abell 2744[3] and Virgo[5], respectively.

RPS is mostly cited for removing the gas needed to form stars, but in doing so it can, on small time scales, induce additional star formation. As the shock front passes through the galaxy it compresses regions of gas and thus kickstarts a burst of star formation. Thus we may be able to observe on-going RPS by identifying instances of small regions of star formation as has been previously observed [3],[4] and simulated [5]. This effect is expected to die out under larger timescales, and thus RPS does retain its title as a quenching process.

Furthermore, (Mulchaey & Jeltema 2010) [6] proposed an additional feature wherein the collision with the over-dense ICM confines any gas outflows due to AGN, supernovae or SF and thus creates an excess of hot gas (measured in the X-ray). Without the normal influx of cold gas, as a field galaxy normally receives, an in-falling cluster galaxy quickly depletes its cold gas reservoir. This starvation induces a shorter lifespan for a galaxy’s star formation and could potentially explain the elliptical abundance observed in nearby cluster centers [1]. While simulations [7] show only a 16% favor for confining ICM interaction, this is an effect which does have a small and perhaps non-negligible influence.

In any case, the debate over the physical mechanism hinges on the existence of a notable distinction between group galaxies and field galaxies. If we note a similar evolution history for galaxies within groups and in the field we may conclude that the processes observed in the more dramatic nature of clusters are indeed unique for the cluster regime. There may be a minor effect wherein RPS plays a small role, but other processes such as confinement are negligible.

The tendency for galaxies to become quiescent upon infall into both groups and clusters is well observed [8], but the prevalence of various driving mechanisms depends on the nature of how these galaxies are quenched.

I.2 Measuring star formation

In order to answer these questions we must have some method by which to measure star formation. As a galaxy forms stars, it begins with massive, OB-type stars which burn at high temperatures for a short amount of time. This high effective temperature corresponds to short wavelength emissions, specifically in the UV. The short lifespan of these stars makes these stars an accurate tracer of recent star formation. Thus in order to probe star formation we may observe a galaxy in a UV (or near UV) filter and associate clump detection with regions of ongoing star formation.

The scale of such clumps of star formation is generally substantially smaller than the size of the galaxy so such analysis requires the galaxy to be finely resolved. This is achieved through either nearby galaxies with low-resolution telescopes or high-resolution telescopes such as HST for distant galaxies. With such an instrument we may probe the fine structures of a galaxy's morphology to analyze the effect of the group environment on these regions of increased star formation.

Part of the expected evolution history which we may observe in these galaxies is the morphological transformation due to tidal forces within the increased gravitational potential [1]. Thus we need some tool which enables us to both quantify morphologies and identify disturbances of "regular"

distributions. GALFIT [9] provides modeling and calculation of sérsic index and radius, as well as a suite of other components.

We may use the sérsic index [10] of galaxies to classify their morphology along the Hubble sequence in order test whether the group potential well has perturbed morphologies in an appreciable way. The sérsic index measures how quickly a galaxy's light profile falls off at extended radii. Within the scope of gas stripping, the effective removal of light from the disk via RPS or some other mechanism induces a much steeper drop off between the bright core and the increasingly dim disk and halo. Thus we may quantitatively compare how effective quenching mechanisms in different regions by comparing sérsic indices.

Additionally, we follow the analysis of (Roediger et al. 2011)[11] and (Tamura et al. 2000)[12] in their use of color gradients in assessing structural history for galaxies in Virgo and the Hubble Deep Field, respectively. They find strong evidence that metallicity (rather than age) gradients account for observed gradients in color. Color gradients provide details about how these metals are distributed, specifically if there is some radial preference. That is to say if metals are preferentially created in an outside-moving-in mechanism. We too use this analysis to identify what role (if any) the group environment has on such metallicity inequalities. The process of group infall may influence how a galaxy creates these metals, and specifically where within spatial distribution this creation occurs, specifically at the redistributive hand of RPS.

CHAPTER II
METHODS

II.1 Data

The subject of this investigation is supergroup (SG) 1120 (hereafter SG1120), an ongoing merger of four groups into a Coma-like cluster at $z = 0.37$ originally discovered by (Gonzalez et al. 2005) (hereafter G05) [13]. It is approximately 14'x9' across and is composed of over 170 spectroscopically confirmed members [14]. Samples RGB images are included in Fig.II.1.

G05 observed SG1120 via *Chandra* ACIS-I in the 0.8-3 keV band. Analysis of this x-ray determined that 4 of 6 sources were bound and calculated a mass of at least a third of the Coma cluster. Their work finds that these four groups are beginning the first stages of filamentary collapse and present several arguments that these structures are indeed bound. Thus SG1120 serves as a clear intermediary between the cluster and group regimes: it is composed of several groups and has hitherto evolved under these circumstances but is on the cusp of merging a massive cluster

We utilize data from the Advanced Camera for Surveys (ACS) (WFC channel) and the Wide Field Camera 3 (WFC3) (UVIS channel) aboard HST with pixel scales of 0.05"/pixel and 0.04"/pixel, respectively. Our filter set includes F390W (WFC3), F606W (ACS), and F814W (WFC3), forming nearly complete coverage from 310nm to 950nm, specifically including the Hα line at 656nm- the identifying feature of HII regions. Group members are apparently distinct from field galaxies within a color-magnitude diagram (Fig. II.2) as we should expect for this collection of objects at a unique redshift amongst the field. The mosaic is displayed in F814W with a RGB (F814,F606W, F390W) overlay for a single group center in Fig. II.3.

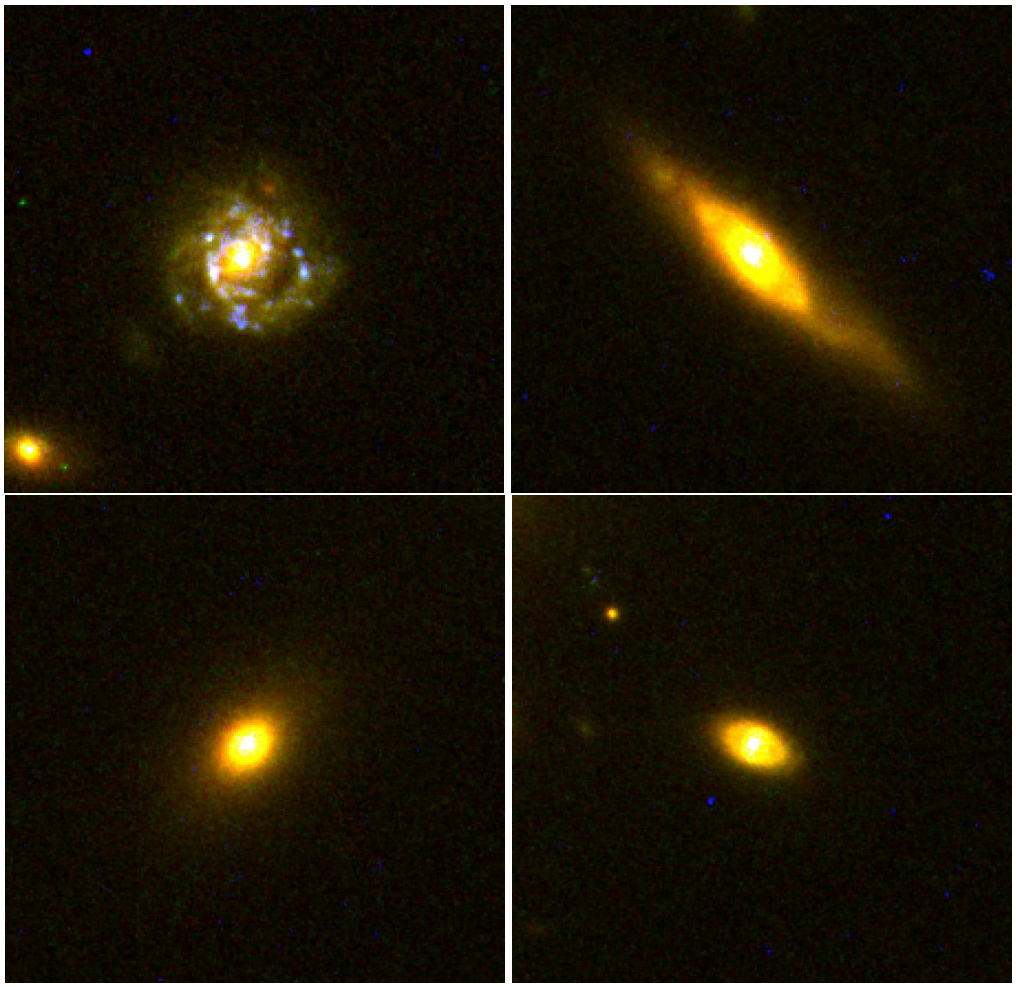

Fig. II.1. RGB (F814W, F606W, F390W) thumbnails of four sample group members. From top left to bottom right, z= 0.369, 0.374, 0.372, 0.370

II.2 AstroDrizzle & TweakReg

The extraordinarily fine pixel scale of WFC3 is necessary in order to resolve fine-scale structures such as individual HII regions. Thus we resample ACS data (pixel-scale 0.05") to the native pixel scale of WFC3 (pixel-scale 0.04") through STScI's AstroDrizzle pipeline [15]. Additionally, we adjust alignment and orientation so that output frames from different filters and passes have the same orientation (North up, East left) and coincide in both WCS and pixel-space. This alignment is crucial for use of SExtractor in dual-image mode.

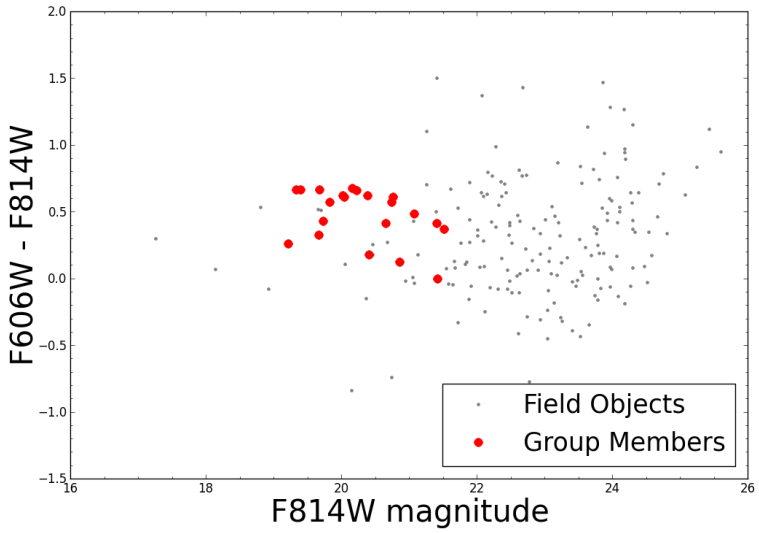

Fig. II.2. Color magnitude diagram of a single group (farthest East in Fig. II.3). Grey points are field objects and red circles are spectroscopically confirmed members.

This procedure further allows us to correct substantial astrometry errors which were present in the data by aligning a variety of orientations and correcting for chip distortions which are present in each instrument. This correction is achieved through default use of TweakReg.

We ran AstroDrizzle with non-default final_scale and final_ref_image. Final_scale controls the output pixel scale, and final_ref_image uses a given reference image to constrain output orientation. Altering final_scale too much introduces additional sources and apparent image holes. This arises from AstroDrizzle's inability to recognize input pixels as the same source when the pixels from respective dithers are separated too much. The image holes are clearly seen as individual pixels within a clear source which are very much lower than surrounding source pixels and much closer to sky values. Visual inspection of each of our output frames reveals that we have not reached this threshold in our conversion from 0.05 ”/pixel to 0.04 ”/pixel.

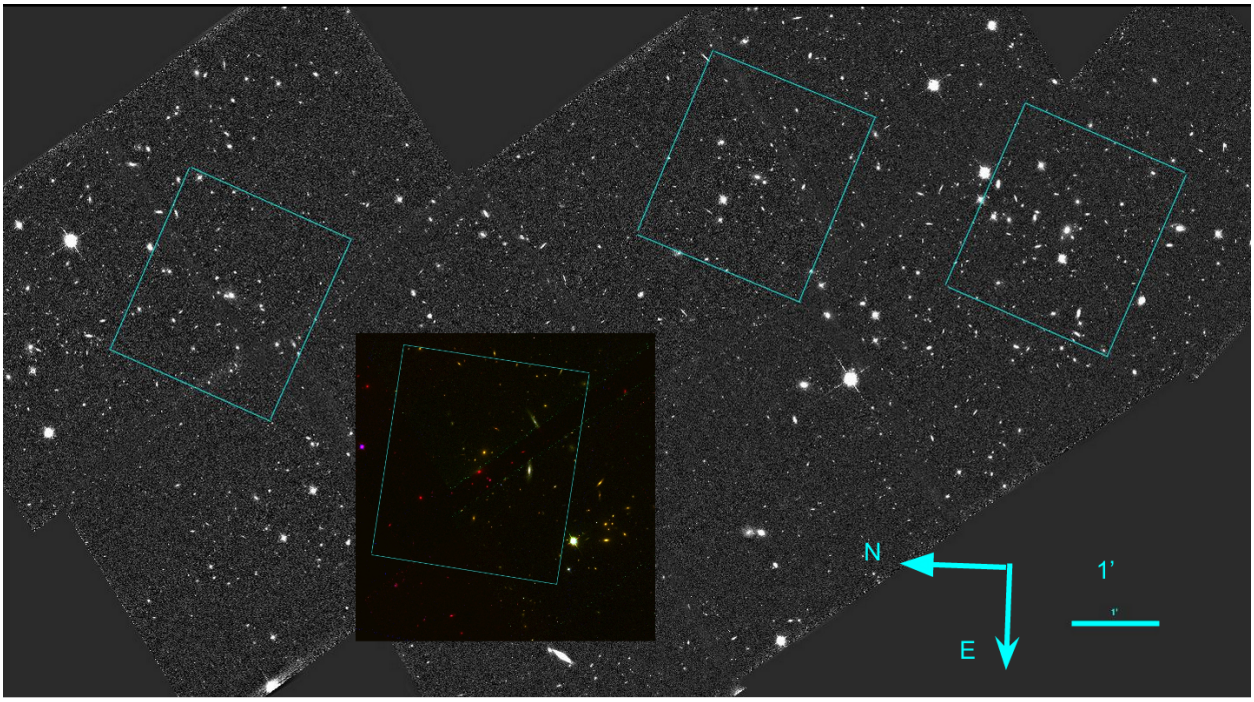

Fig. II.3. The full mosaic in F814W with boxes about group centers with RGB (F814W,F606W,F390W) overlay of each group. 1' is shown in bottom right. Note North is to the left and East is down.

AstroDrizzle outputs weight maps according to its resampling and drizzling procedures, however the format is inappropriate for our later tasks. We thus correct these maps to an RMS format according to the procedure laid out by (Casertano et al 2000b) [16] according to $\frac{F_A}{\sqrt{\text{Drizzle weight}}}$, where

$$\sqrt{F_A} = \begin{cases} \frac{s}{p}(1 - \frac{s}{3p}), & (s < p) \\ (1 - \frac{p}{3s}), & (p < s) \end{cases} \tag{II.1}$$

II.3 SExtractor

We utilize SExtractor [17] to calculate basic photometry (magnitude, half-light radius, etc) and fixed aperture photometry. After a sky cut SExtractor identifies sources via iterative sigma-clipping and calculates photometry by calculating flux within calculated and/or given isophotes.

In order to guarantee consistent aperture sizes we run SExtractor in dual-image mode wherein one image is used for detection and the other is used for calculations. We choose our reddest filter, F814W, to serve as the reference image so that all sources are included. We adjust the instrument and filter-specific zeropoints, saturation levels, pixel scales and seeing FWHM. Additionally, we use a Gaussian filter to smooth imaging before image detection to increase our faint object detection.

In order to identify data quality we use these initial calculations to identify curve of growth tendencies for several bright, non-saturated field stars (Fig. II.4). As expected, these have a steep flux increase before sharply flattening out as apertures extend to larger radii. This result indicates that there is no excess diffusion of pixels and that the point spread function is sufficiently well-behaved.

II.4 GALFIT & PyMorph

GALFIT is modeling software which simultaneously fits two-dimensional radial light profiles of multiple components to a variety of galaxy structures and morphologies. We utilize the same zeropoints and pixel scales as with SExtractor and input SExtractor's calculations of magnitude, half-light radius, position angle, and sky flux as initial guesses. Furthermore, we invert (1's to 0's and vice versa) SExtractor's segmentation map for use as a bad pixel mask. Except for zeropoints and pixel scales, we allow GALFIT to vary each of the these in order to fit models with a variable Sérsic index. GALFIT outputs its best-fit model along with the residual product when the model is subtracted from the original. We use GALFIT's reduced χ^2 calculation as an error estimate after visually inspecting the residual product.

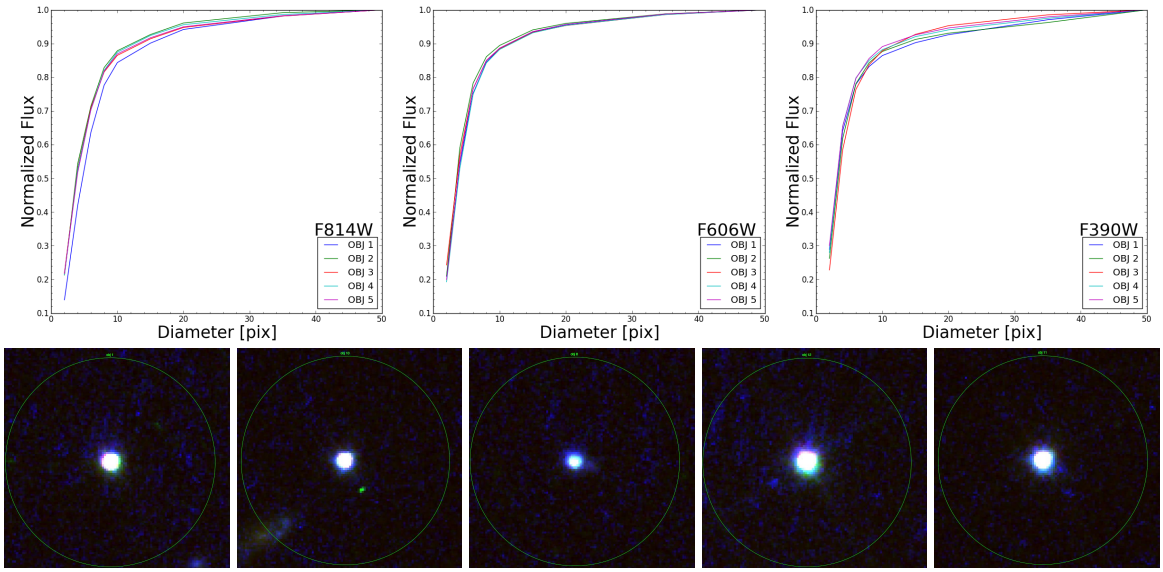

Fig. II.4. Curve of growth curves for several bright, non-saturated stars in (left to right) F814W, F606W, F390W. Note the sharp increase and flat extension. RGB (same order) thumbnails are included below with largest aperture as green circle.

PyMorph aims to create a collective package of galaxy fitting, incorporating SExtractor, GALFIT, and its own additional modules to fully model galaxies and classify their morphologies. It is an impressive undertaking, but in order to maintain a degree of flexibility and our control of individual calculations we opt to isolate portions of PyMorph and use GALFIT's solutions as input. We extract components to calculate Gini Coefficient (G) and the second order moment of the brightest 20% of pixels (M_{20}), using GALFIT's calculations of central coordinates, axis ratio, position angle, sky-value and associated errors.

II.5 Parameters

Following the standard magnitude system we use published zeropoints for the respective filters of ACS [18] and WFC3 [19]. Because HST is located in space these zeropoints remain constant over time and are independent of atmospheric conditions [20]. These characteristics allow for regular

use of the conversion from flux to magnitude in each filter according to Equation II.2, where m_0 is the reference magnitude (zeropoint) and F_0 is the reference flux (1 $e \cdot sec^{-1}$)

$$m - m_0 = -2.51 \cdot log(F/F_0) \tag{II.2}$$

A galaxy's Sérsic index, n, measures the severity of its radial light-profile drop-off. More precisely, it is the power of the exponential term in Equation II.3 which describes a galaxy's intensity as a function of radius. Spiral galaxies tend towards higher Sérsic indices while elliptical tend towards lower ones. On average, however, Sérsic indices for elliptical galaxies average around 4, i.e. a de Vaucouleurs profile. Sérsic indices of cluster galaxies tend towards lower values as a result of the gas stripping and mergers which disassociate extended structures such as spiral arms and other high Sérsic index characteristics [1]. As a result, we search for this same tendency within SG1120 to identify whether the group environment is capable of such transformation.

$$I(R) \propto e^{-kR^{1/n}} \tag{II.3}$$

We use color gradients to quantify how star-formation features are distributed across all radii. Age and metallicity gradients are degenerate causes of color gradients, but we are nonetheless able to derive galaxy characteristics from these calculations. Regardless of the cause, color gradients provide insight into a stellar population's evolution- namely whether and where new stars have been recently or vigorously produced (age or metallicity, respectively). As more pronounced gradients indicate older and more metal rich inner regions we can quantify the spatial-distribution of novel star-formation. We expect that the influence of the IGM on in-falling galaxies would induce novel star-formation in regions throughout the galaxy thereby enriching the outer regions and displaying a color gradient.

Our color gradients are calculated from a variety of fixed apertures based on nearness to a quarter, half, full, double and triple half-light radius. This range of values was selected to maintain reliable results at outer radii while still enabling us to probe the innermost structure of each galaxy. In the calculation we subtract flux measurements of apertures to get flux gradients within each annuli and take the log of the ratio to get a color gradient in both U-I and V-I, while propagating the original flux uncertainty accordingly.

For flatter gradients red emission dominates throughout all radii. This is typical of larger galaxies with high mass and high luminosity. If induced by metal gradients, these flat gradients indicate that metals are evenly distributed throughout the galaxy after a sufficiently long mixing period. The long time-span which this process requires implies that the galaxy is old and its star formation is static. If these gradients are instead produced by age gradients then a flat results indicates the same- the galaxy is sufficiently old to possess an equilaterally old stellar population. Steep gradients, however, indicate a red-dominated core and bluer extended regions. This feature is characteristic of spiral galaxies which are characterized by the increased star-formation within extended arms at large radius. Positive gradients appear in moderation for galaxies with blue cores where star-formation has a burst of activity and quickly fades. These systems only live around a billion years and have been found in lower-density environments [21]

CHAPTER III
RESULTS

III.1 Morphological Transformation

After performing basic correctness analysis we draw first order conclusions about observed morphologies. Based on visual classification we find that the majority of spiral galaxies are preferentially located on the outer rim of the group. Galaxies which are well detected in all filters and not polluted by edge effects are included in a contact sheet of RGB thumbnails in Figure III.5.The relatively recent supergroup formation history [13] indicates that these periphery galaxies have probably not made their first pass through the group center. Thus they have neither had time to interact with the IGM nor have been in a high-density environment which would be most effective in transforming these galaxies into the elliptical of the centrally-located galaxies.

We find that the majority of group members have elliptical morphologies. As a typical example, m1b.KS06.B-635 (Figure III.1, upper left) resides 32" from the group center and has a clear elliptical structure. This distance appears to be within a core region that extends to around 40" (see Figure III.3 and ignore the y-axis). All but one galaxy in this region display elliptical morphologies, consistent with our claim that at least the group core has an effect on galaxy morphology. The outlying spiral is discussed below.This result comes as no surprise given past work which has shown the majority of galaxies throughout the field, groups and clusters tend towards ellipticals [1].

Several instances of these spiral digress from this pattern. Although not as clear as other examples, vim-20982 in Figure III.1 (upper right) does exhibit spiral characteristics. After constructing the RGB composite, its spiral nature is more easily distinguished when interpreted as an edge-on spiral with signs of inter-arm gaps on the southwest corner. We find this galaxy at a distance of 88", a bit outside the median projected distance, 83". At this distance from the group center we may expect

a moderate amount of induced star formation and morphological changes via interaction with a modest increase in the IGM density. We cannot tell through morphology alone, however, whether this comes from its interaction with the IGM or from its uninfluenced evolution.

m4b.KS06.B-795 (Figure III.1 lower left) is further outside the mean distance at 100" and contains a proto-spiral structure with a stark lack of star formation. These intriguing characteristics indicate that although it is nearly within the median distance to the BGG it has maintained this pristine and delicate collection of non star forming spiral arms. Again, morphology alone cannot distinguish whether this is merely a projection effect or if there is something more intriguing about this member.

m4a.KSF2-0961, Figure II.1 (lower right) is located 121" from the BGG, and possesses clear spiral arms with an abundance of star formation. The high star formation is typical for such a galaxy which has likely spent the majority of its life passively evolving in the field. There are no signs of major disturbances in its morphology further indicating that it is a recent addition to the group.

Oddly enough, it appears that there is an additional spiral in the center of the group, 9" from the group center. This could be an in-falling galaxy whose star-formation has been greatly enhanced from IGM interaction, but we are unable to eliminate projection effects. It also falls within the incomplete imaging section of our F606W data so we cannot make any complete claims about its structure or history.

The BGG of this central group has evidently not remained in such an undisturbed state. It contains two clear and distinct cores- evidence of a recent major merger. This partially confirms the similarity between groups and clusters. The observed hierarchical nature of BCG evolution via major mergers [22] has a similar effect in this group.

Fig. III.1. RGB (F814W, F606W, F390W) thumbnails highlighting particular morphologies. From top left to bottom right: m1b.KS06.B-635, vim-20982, m4b.KS06.B-795, m4a.KSF2-0961. Same order, distance from BGG: r = 32", 88", 100", 121". The residual green splotches are a result of chip edge effects. North is up and East is to the left.

III.2 Distance Dependences

In order to better determine the influence of environment on member galaxies we search for correlations between certain factors and the distance to the group center. Were the group environment influential in these regards we should expect trends of more pronounced effect as galaxies tend to-

wards the center of the group where higher IGM density, greater merger probability and increased in-fall velocities enhance these transformations.

III.2.1 Sérsic indices

In an effort to better quantify the detailed effects of this merging system we calculate sérsic indices in F814W for the majority of member galaxies. We neglect 10 members which lie near or outside of our chip boundaries. As these galaxies fall into the group center, we expect that their outer gas would be striped leaving only the dense core and other central, compact components. This dispersion effect would systematically increase sérsic indices as the core begins to substantiate a larger percentage of the galaxy. Yet when we correlate sérsic index with distance in Figure III.2, we find no relationship between the two. Indeed, by sigma-clipping ($\sigma = 0.97$) our calculations and refitting a least-squares we find the slope changes from negative (-0.003) to positive (0.001), further indicating no relation.

We note, however, that the majority of our calculations are not characteristic of the values we expect for the majority of galaxies. De Vaucouleurs profiles are the most typical finding for most galaxies. With any trend we expect to find it rotated about n=4, yet our data seems to have a systematic shift lower than this expected value. Whether correcting this offset would merely shift all points up and thus maintain the correlation or if it would effect all points randomly is unknown. This unexpected results adds to the variety of arguments which comes against this claim that this group environment as had a perceptible effect sérsic indices of members.

III.2.2 Color at the Core

As galaxies interact with IGM their colors vary with changes in star formation. To distinguish whether this has a quenching or enhancing effect we plot color (both U-I and V-I) within 1 half-light radius as a function of distance in Figure III.3. Neglecting possible outliers due to projection

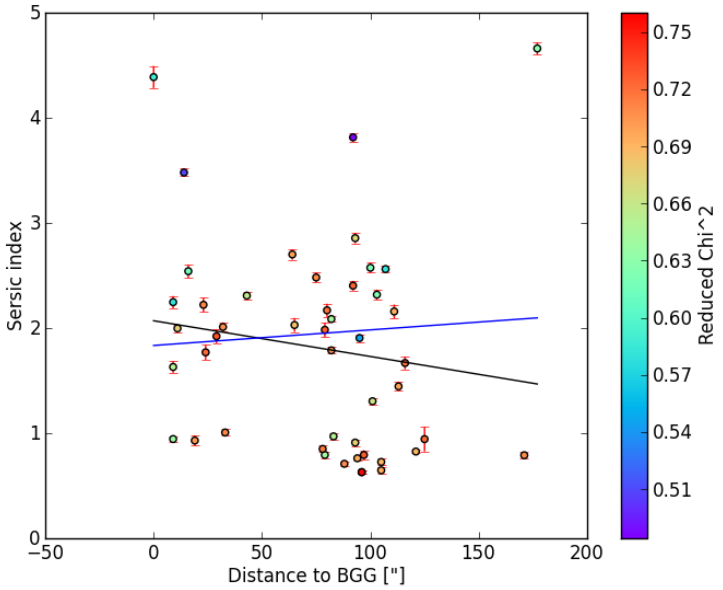

Fig. III.2. GALFIT's calculation of the sérsic index plotted against the distance to the group center. Included as a heat map is GALIFIT's reduced χ^2 calculation. We excluded 10 members which were either near chip boundaries or outside our imaging range. We note that there is no significant trend, and that these values differ substantially from the expected de Vaucouleurs profile. The black line is a least squares fit (slope -0.003) and blue line is sigma-clipped ($\sigma = 0.97$) least squares with slope 0.001.

effects, we notice a slight yet significant trend in U-I color as function of distance. This implies that the group core is notably redder than the general population, indicating a tendency for quenching in the higher density regions as observed in cluster environments. We do not observe a similar correlation in V-I, however. Although it has a moderately low standard deviation (0.25) this trend only shows a slight reddening with nearness to BGG. The slightness of the slope (-0.001) over such a range of distances also makes this result more likely a statistical coincidence rather than evidence for a physically driven process like RPS.

We interpret the combination of these results has evidence that SG1120 has had slight, but effective, influence over the reddening of member galaxies. Clusters frequently demonstrate this

characteristic, having red-dominated, largely quiescent galaxies at their cores. We emphasize that our calculation is done on the core of each galaxy and thus does not speak to the effect of the group environment on the outer regions of galaxies.

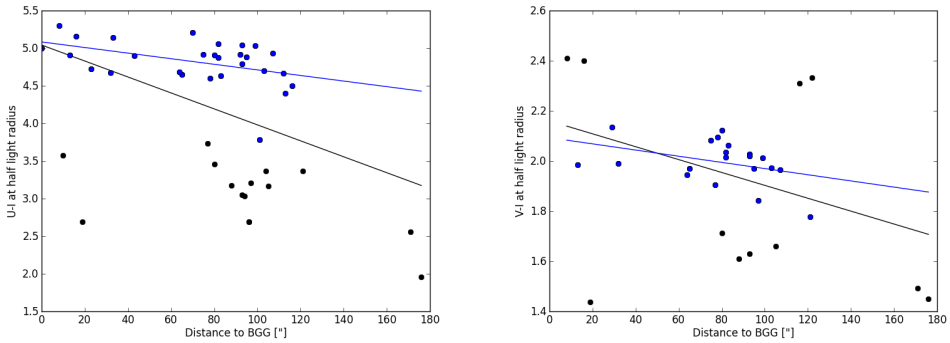

Fig. III.3. Color at aperture of 1 half-light radius in U-I and V-I vs Distance to the BGG. We note no significant trend. In each U-I and V-I, the black line is a least squares fit with slope -0.010 and -0.003, respectively. Blue points are within a standard deviation (U-I: $\sigma = 0.92$, V-I: $\sigma = 0.25$) and the blue line is the corresponding sigma-clipped least squares fit with slope -0.004 and -0.001, respectively.

III.2.3 Color Gradients

Throughout our sample we find multiple instances of both steep and flat gradients, however, they collectively tend towards flat and almost exclusively negative values indicating a majority of red-dominated or older galaxies. This is not unexpected given both the likelihood of attenuation via dust and the normalcy of flat gradients for elliptical galaxies. A contact sheet with calculated color gradients of galaxies which are detected in all filters are included in Figure III.6 for U-I and Figure III.7 for V-I. Due to a gap in F606W pointings our dataset has a band of incompleteness centered on the group center, and these galaxies are excluded from these Figures.

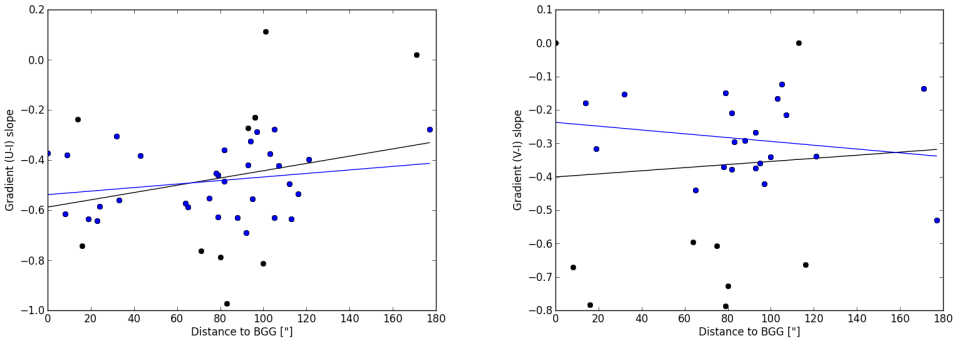

Fig. III.4. Slopes of linear fits to the color gradient of each member (in both U-I and V-I) vs distance from BGG in arc seconds. We note no significant trend. In each U-I and V-I, the black line is a least squares fit with slope 0.0015 and 0.0004, respectively . Blue points are within a standard deviation (U-I: $\sigma = 0.21$, V-I: $\sigma = 0.22$) and the blue line is the corresponding sigma-clipped least squares fit with slope 0.0007 and -0.0005, respectively.

In order to correlate observed color gradients with the in-fall process we calculate a linear fit, weighted by propagated flux uncertainties, for each gradient in order to get a single representative number for each galaxy. When this effective slope is plotted against distance (Figure III.4) we find a lack of meaningful correlation in both U-I and V-I. The least squares fits in U-I and V-I are weakened and inverted, respectively, by a one sigma clip. Both populations also have large standard deviations (0.21 and 0.22) which limits the accuracy of the linear regression. As with previous metrics we cannot claim any kind of physical mechanism has caused these results.

The effect of dust can greatly influence the results of a calculated gradient. The reddening effect suppresses bluer emission and thus tends to lower gradient slopes. A few members in our sample are edge-on and display clear dust lanes with correspondingly low calculated gradients (Figures III.6, III.7, III.5 bottom right corner). In these cases, however, the calculations for edge-on galaxies are inherently more difficult, especially with fixed-aperture photometry and thus these calculations tend to be fairly error-prone.

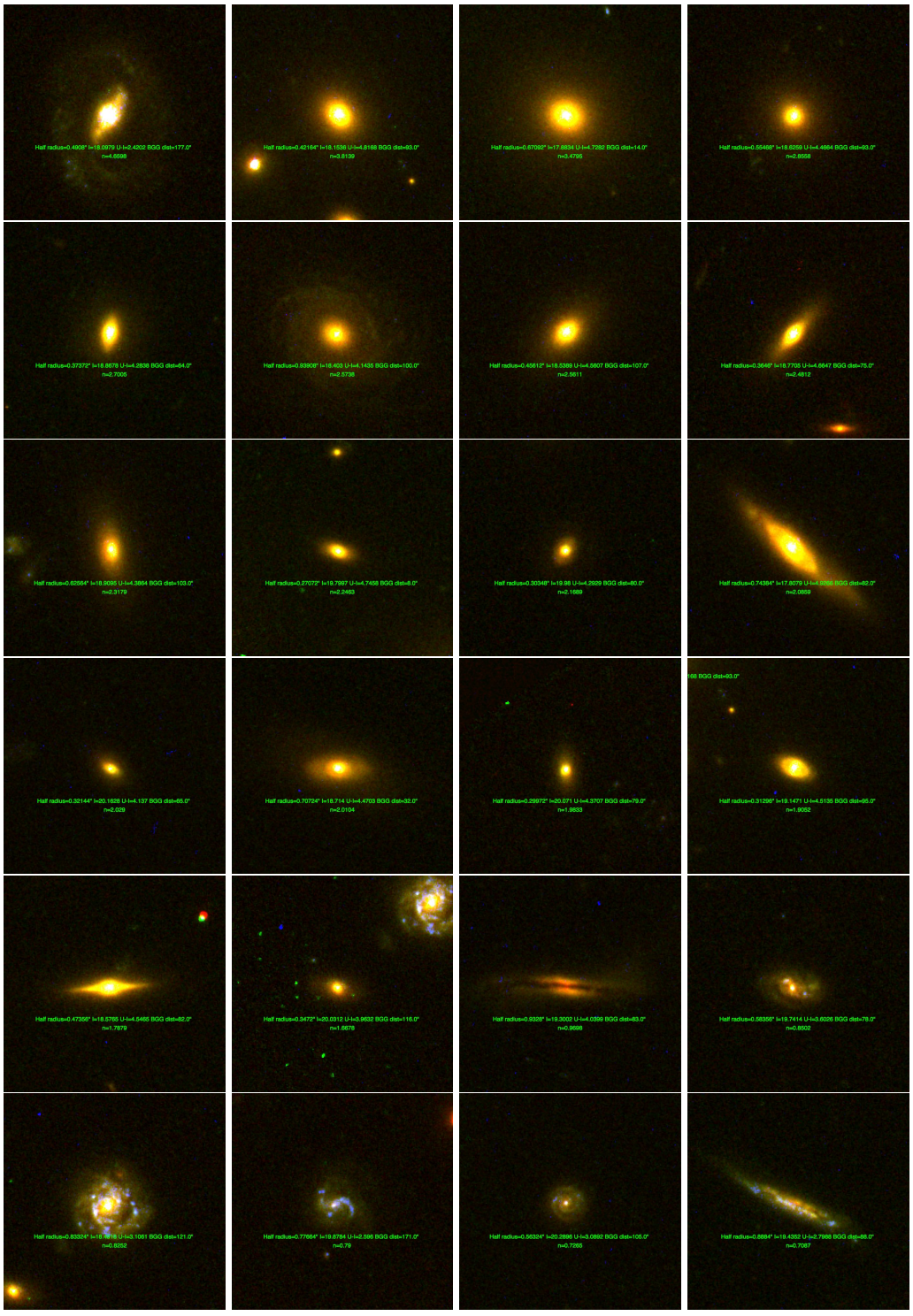

Fig. III.5. RGB = F814W, F606W, F390W composites for all full-band detected images. Order of images is same as Figures III.6 and III.7- highest sérsic index first. Green dots in several images are chip-edge artifacts. North is up and East is to the left.

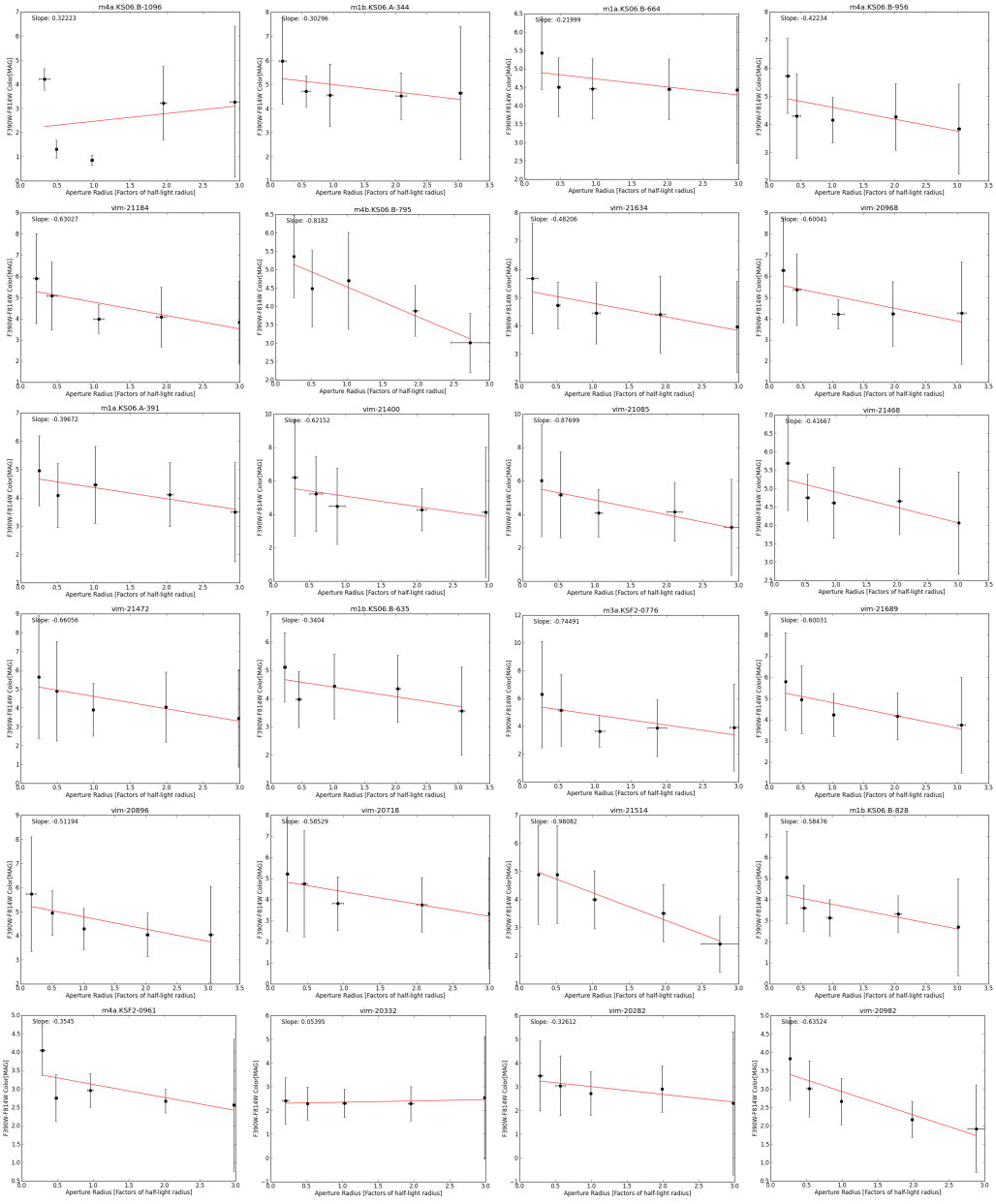

Fig. III.6. Color Gradients in F390W - F814W for full-band detected galaxies. Ordered from highest to lowest sérsic index.

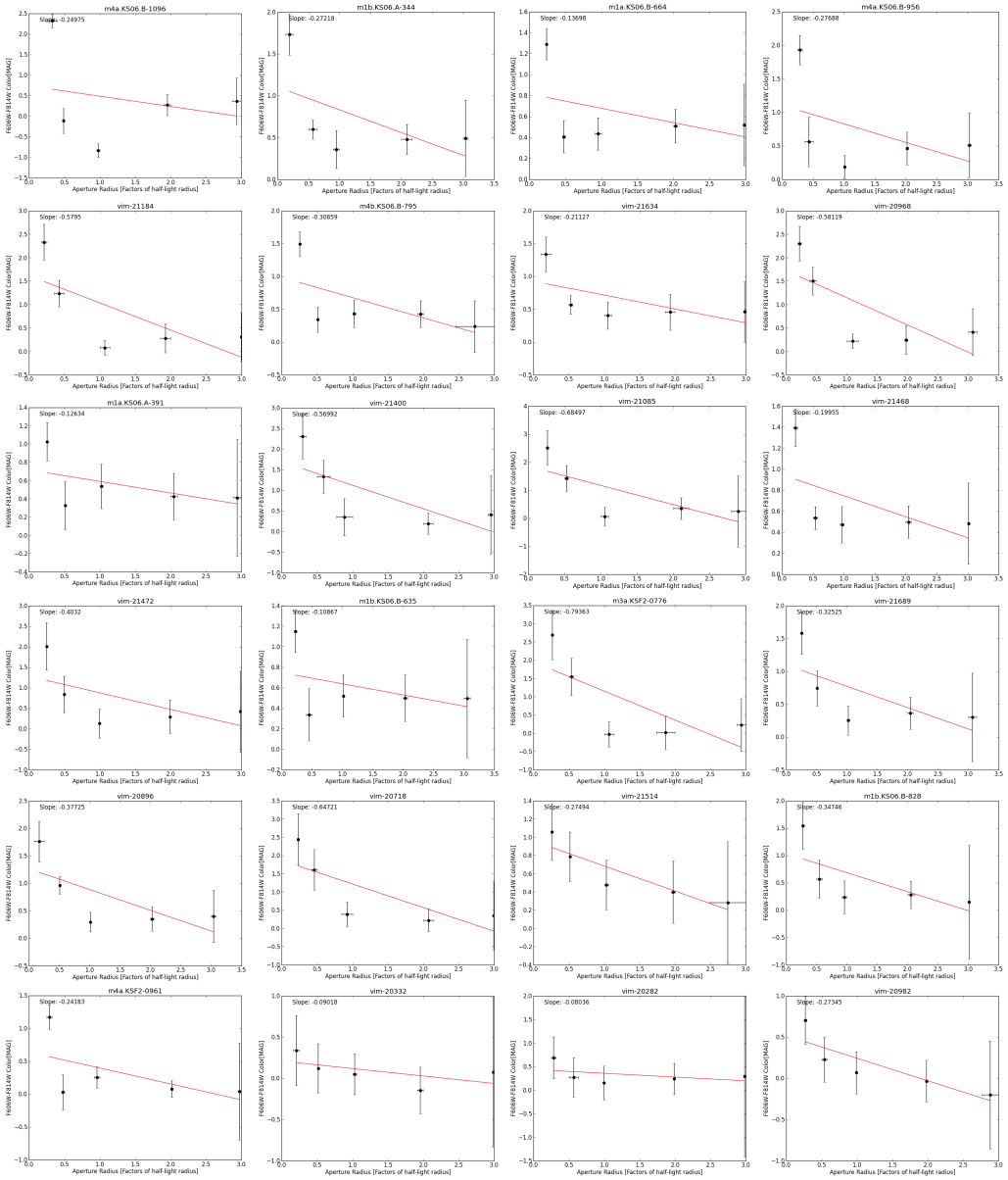

Fig. III.7. Color Gradients in F606W - F814W for full-band detected galaxies. Ordered from highest to lowest sérsic index.

CHAPTER IV
CONCLUSIONS

We have investigated SG1120 as a progenitor of a Coma-like cluster in order to ascertain whether it is able to produce effects observed in higher density and more massive regions of clusters. Observing this supergroup before it transitions into the cluster regime enabled us to make claims about the boundary region between groups and clusters.

Through our metrics of morphologies, sérsic indices, central colors and color gradients, we did not find any substantial correlation with distance to the group center. On the contrary, we found correlations similar to those of clusters where galaxies tend to share a scattered distribution. This suggests that SG1120 has produced a cluster-like environment even in its proto-cluster state. Although we do not observe any examples of the dramatic stripping effects of RPS, we nonetheless have several other measures by which we confirm the integral role of the group regime in cluster evolution.

Our work has been limited to a relatively small sample size, and we would need to expand our data set in order to make broad assertions about all groups. Furthermore, assuming our results hold for more observations, we should like to extend current cluster simulations to include the group regime to more precisely determine the inadequate factor of the group environment.

REFERENCES

1. Moore, B., Katz, N., Lake, G., Dressler, A. & Oemler, A. Galaxy harassment and the evolution of clusters of galaxies. *Nature* **379,** 613–616 (Feb. 1996).

2. Gunn, J. E. & Gott, J. R. III. On the Infall of Matter Into Clusters of Galaxies and Some Effects on Their Evolution. *ApJ* **176,** 1 (Aug. 1972).

3. Owers, M. S., Couch, W. J., Nulsen, P. E. J. & Randall, S. W. Shocking Tails in the Major Merger Abell 2744. *ApJL* **750,** L23 (May 2012).

4. Kenney, J. D. P. *et al.* Transformation of a Virgo Cluster Dwarf Irregular Galaxy by Ram Pressure Stripping: IC3418 and Its Fireballs. *ApJ* **780,** 119 (Jan. 2014).

5. Roediger, E., Brüggen, M., Owers, M. S., Ebeling, H. & Sun, M. Star formation in shocked cluster spirals and their tails. *MNRAS* **443,** L114–L118 (Sept. 2014).

6. Mulchaey, J. S. & Jeltema, T. E. Hot Gas Halos in Early-type Field Galaxies. *ApJL* **715,** L1–L5 (May 2010).

7. Bahé, Y. M., McCarthy, I. G., Crain, R. A. & Theuns, T. The competition between confinement and ram pressure and its implications for galaxies in groups and clusters. *MNRAS* **424,** 1179–1186 (Aug. 2012).

8. Boselli, A. & Gavazzi, G. Environmental Effects on LateType Galaxies in Nearby Clusters. English. *PSAP* **118,** pp. 517–559. ISSN: 00046280 (2006).

9. Peng, C. Y., Ho, L. C., Impey, C. D. & Rix, H.-W. Detailed Structural Decomposition of Galaxy Images. *AJ* **124,** 266–293 (July 2002).

10. Sérsic, J. L. Influence of the atmospheric and instrumental dispersion on the brightness distribution in a galaxy. *Boletin de la Asociacion Argentina de Astronomia La Plata Argentina* **6,** 41 (1963).

11. Roediger, J. C., Courteau, S., McDonald, M. & MacArthur, L. A. The formation and evolution of Virgo cluster galaxies - I. Broad-band optical and infrared colours. *MNRAS* **416,** 1983–1995 (Sept. 2011).

12. Tamura, N., Kobayashi, C., Arimoto, N., Kodama, T. & Ohta, K. Origin of Color Gradients in Elliptical Galaxies. *AJ* **119,** 2134–2145 (May 2000).

13. Gonzalez, A. H., Tran, K.-V. H., Conbere, M. N. & Zaritsky, D. Galaxy Cluster Assembly at z=0.37. *ApJL* **624,** L73–L76 (May 2005).

14. Tran, K.-V. H. *et al.* A Spectroscopically Confirmed Excess of 24 μm Sources in a Super Galaxy Group at z = 0.37: Enhanced Dusty Star Formation Relative to the Cluster and Field Environment. *ApJ* **705,** 809–820 (Nov. 2009).

15. Gonzaga, S., Hack, W., Fruchter, A. & Mack, J. The DrizzlePac Handbook. *STScI,* 63–124 (2012).

16. Casertano, S. *et al.* WFPC2 Observations of the Hubble Deep Field South. *AJ* **120,** 2747–2824 (Dec. 2000).

17. Bertin, E. & Arnouts, S. SExtractor: Software for source extraction. *AAPS* **117,** 393–404 (June 1996).

18. Mack, J., Gilliland, R. L., Anderson, J. & Sirianni, M. WFC Zeropoints at -81C. *STScI-ISR* **ACS,** 1 (May 2007).

19. Kalirai, J. S. *et al.* WFC3 SMOV Proposal 11450: The Photometric Performance and Calibration of WFC3/UVIS. *STScI-ISR* **WFC3,** 1 (Nov. 2009).

20. Kalirai, J. S., Baggett, S., Borders, T. & Rajan, A. The Photometric Performance of WFC3/UVIS: Temporal Stability Through Year 1. *STScI* **WFC3,** 1 (Oct. 2010).

21. Suh, H. *et al.* Demography of Sloan Digital Sky Survey Early-Type Galaxies from the Perspective of Radial Color Gradients. *ApJS* **187,** 374–387 (Apr. 2010).

22. De Lucia, G. & Blaizot, J. The hierarchical formation of the brightest cluster galaxies. *MNRAS* **375,** 2–14 (Feb. 2007).